3444

3444

Laboratory Flow Characteristics Of Gun Perforations

W. T. Bell, SPE-AIME, Schlumberger Well Services
E. F. Brieger, SPE-AIME, Schlumberger Well Services
J. W. Harrigan, Jr., Schlumberger Well Services

Introduction

From the inception of the gun perforating technique in 1932, the ultimate test of perforator effectiveness has been well productivity. As a result, much attention has been devoted to laboratory testing of perforators as a means of predicting and improving well performance. Laboratory procedures have evolved over the years from simple single-shot penetration tests in steel to multishot tests in large cement targets using actual field guns. Shots at atmospheric pressure have been supplemented with tests under pressure and temperature environments simulative of down-hole conditions.

Interest in laboratory flow properties of perforations entered the picture in 1953 with the introduction of the laboratory flow test.[1] This test, refined in 1956,[2] culminated in the standard API RP 43 procedure in 1962.[3] The API procedure until recently used Well Flow Index (WFI) as a means of comparing flow performance of perforations in the linear-flow system employed. However, no true indication of the productive capacity of a perforation in the more nearly radial flow system that is encountered down hole could be derived from the WFI measurement.[4] In an effort to provide more meaningful data, the API procedure was revised in 1971 to introduce Core Flow Efficiency (CFE) as the indicator of laboratory performance in the linear target.[5] CFE is the ratio of flow from an actual perforation to flow from an ideal perforation of the same diameter and depth in the same target. While CFE represents a better basis than WFI for comparing perforation performance in the laboratory, the linear nature of flow in the API target still has raised questions as to the validity of applying CFE to down-hole conditions.

Consequently, studies were undertaken to better define the liquid-flow characteristics, and particularly the flow efficiencies, of perforations under conditions more simulative of those down hole. Calculated flow and pressure distributions surrounding single perforations in linear laboratory targets were compared with those existing around single perforations in a simplified down-hole model. Perforation-flow efficiencies for the down-hole model were calculated and confirmed in simulative experimental tests.

Pressure and Flow Distributions— Ideal Perforations

Mathematical models of the linear target and a simplified down-hole system were developed to facilitate investigation of the flow and pressure distributions in the two systems. Initial work was done on ideal perforations since their flow rates are the basis for calculating perforation-flow efficiencies.

The mathematical approach employed in analyzing the linear target is commonly referred to as the finite-difference technique. The target model is divided into a series of concentric segments as shown in Fig. 1. Using Darcy equations for radial and linear flow in porous media,[6] expressions are written for the pressure in each segment as a function of the pressure in

Flow rates through gun perforations calculated for radial-flow conditions and confirmed in laboratory tests indicated perforation efficiencies substantially lower than those observed in API RP 43 tests with linear-flow test targets. Observed perforation efficiencies were also strongly influenced by differential pressure: below the API RP 43 standard of 200 psi, efficiencies were significantly decreased.

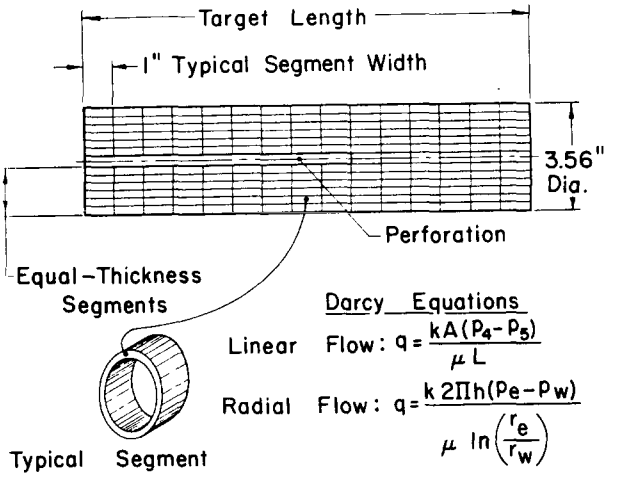

Fig. 1—Model of linear laboratory system.

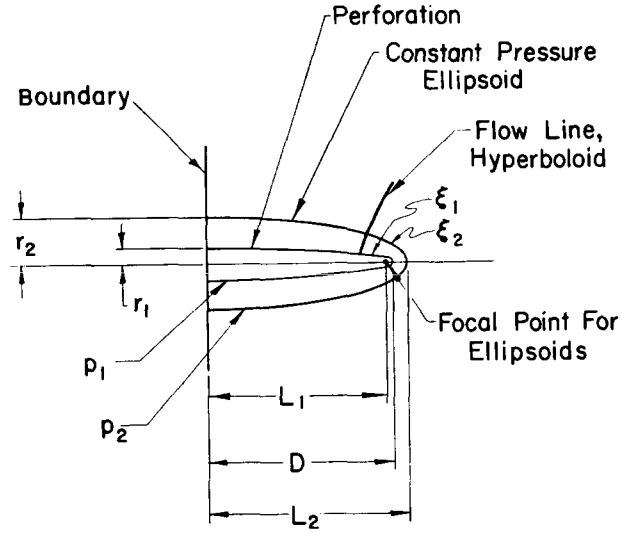

Fig. 2—Model of simplified down-hole system.

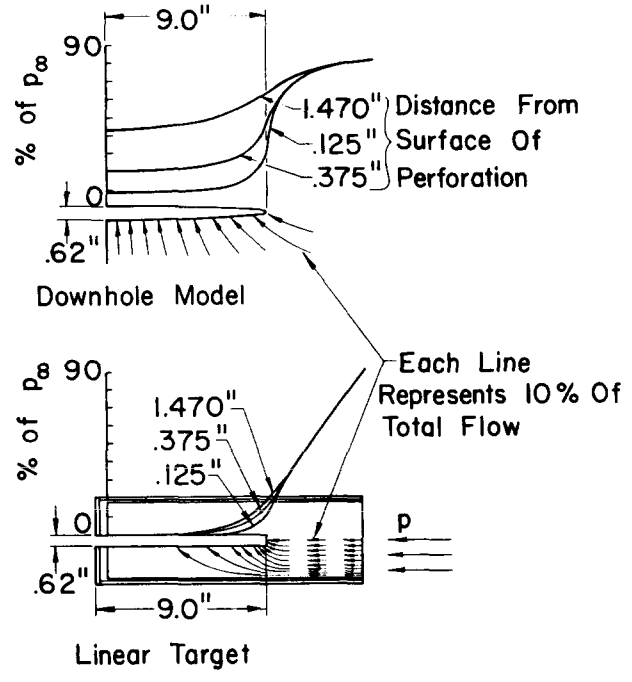

Fig. 3—Flow and pressure distributions—ideal holes.

the four segments immediately adjacent. The resulting system of equations is solved to determine the pressure in each segment. Using the calculated pressures, the flow rates into and out of each segment are determined from the Darcy relationships.

The mathematical model selected to simulate the down-hole system is represented by a single half-ellipsoidal perforation extending from a plane boundary surface into a semi-infinite porous medium (Fig. 2). This simplified approach, which neglects the effects of shot density and phasing, permits rapid analysis of flow characteristics of a number of combinations of perforation diameter and depth. Pressure distributions around the ellipsoidal perforation are represented by a series of coaxial ellipsoids, each of which has a constant pressure along the surface. Flow enters the perforation along a series of coaxial hyperboloids. The expressions for the pressure along any ellipsoid and the total flow entering the perforation are given by Eqs. A-1 and A-2, respectively, in the Appendix.

Calculated flow and pressure distributions for a typical ideal perforation in the linear and down-hole perforation models are shown in Fig. 3. The differences are striking. Pressure along the perforation in the down-hole model is essentially uniform and substantially higher than that in the linear model. Flow entering the perforation in the linear model is concentrated in the portion of deepest penetration of the hole, whereas that in the down-hole system is distributed uniformly along the perforation. The flow distributions shown in Fig. 3 for the linear target are not greatly altered by changes in diameter or depth of ideal perforations. Total flow rates from perforations in the down-hole model are significantly higher than those from perforations in the linear system, as indicated by Fig. 4.

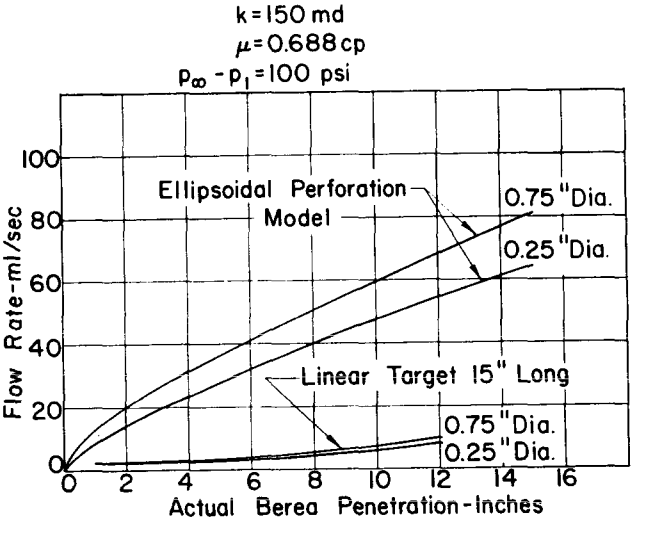

Fig. 4—Flow rates for linear and down-hole models.

The calculated data for the linear model were verified experimentally using standard API RP 43 sandstone targets containing drilled perforations of various diameters and depths. Measured flow rates agreed within 10 percent of the calculated rates.

Experimental verification of the down-hole model involved the use of the standard API Berea core with flow entering radially as shown at the bottom of Fig. 5. It can be seen that this system is similar to the ellipsoidal perforation model illustrated at the top of Fig. 5. The pressure imposed on the cylindrical core was the same as that determined for the ellipsoidal model (Eq. A-1 in Appendix) at a radius, r_2, equal to the core radius. Measured flow rates from drilled perforations in cylindrical cores agreed within 6 percent with rates calculated using the ellipsoidal model.

The calculated flow and pressure distributions indicate that the linear system is not simulative of the specific down-hole conditions assumed. However, the data are based on ideal perforations. Shot perforations are not ideal as indicated by CFE's ranging from 0.65 to 0.85 for various perforators. The low CFE's apparently result from a reduced-permeability zone of crushed and compacted stone surrounding the perforation.

Influence of Crushed Zone

Although the presence of this crushed or compacted zone has been known for some time,[1,2] the implications of its presence have not been fully understood. The damaged area is created by the extreme pressures emanating from the shaped-charge jet. A substantial amount of the disturbed material remains even after the perforation has been flowed extensively. A similar crushed zone is observed around bullet perforations.[1,2]

Because of serious difficulties experienced in obtaining reliable physical measurements of the crushed-zone permeability, the permeability was estimated using the linear mathematical model. This involved superimposing measured compacted-zone configurations on the model and assuming a constant reduced permeability within the damaged area. For these calculations, the boundary of the compacted zone was taken as the limit of obvious disturbance of the cementation between the sand grains in the Berea target. Extent of the zone for typical perforations is shown in Fig. 6. Perforations with CFE's of about 0.75 were found to have crushed-zone permeabilities that were only about 10 to 20 percent of the permeability of the undisturbed stone.

To determine the influence of the crushed zone on flow rates and pressure distributions it is necessary to modify Eq. A-1 as shown in Eq. A-3 in the Appendix. The system assumes a crushed zone of uniform thickness in ellipsoidal coordinates. The flow rates are also readily calculated as shown in Eq. A-4 in the Appendix.

To investigate possible changes in flow distribution resulting from the presence of the crushed zone, the finite-difference technique was applied to the radial model shown in Fig. 5, but with crushed zones similar to those shown in Fig. 6 superimposed. The method used was similar to that employed earlier for the linear model.

In both the linear and radial systems the presence of the crushed zone tended to rearrange the flow distributions within the target, but the basic difference between the linear and radial models remained essentially unchanged. Flow was still concentrated in the end of the perforation for the linear model and was essentially uniform along the perforation in the radial system. The most significant finding was that the calculated flow rates from perforations with typical crushed zones in the radial system were only 25 to

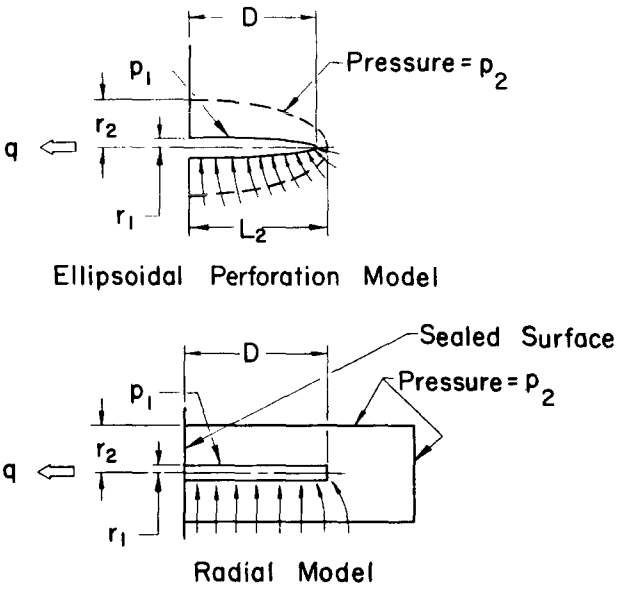

Fig. 5—Radial-flow models.

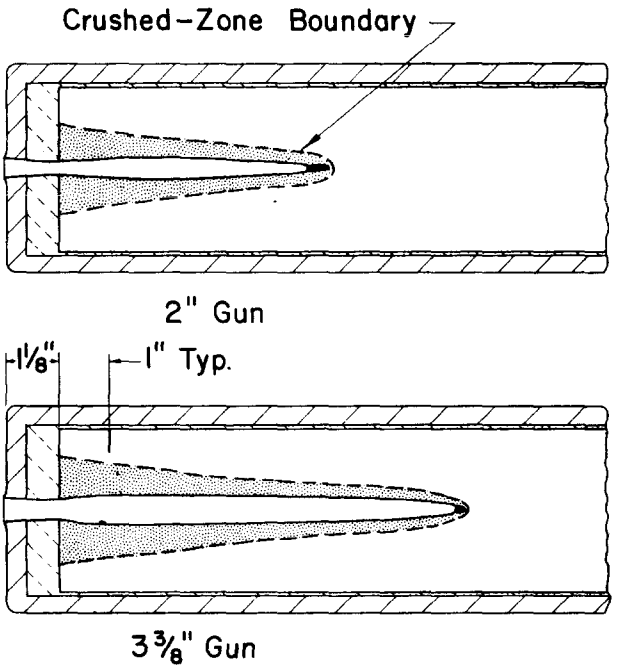

Fig. 6—Typical perforation configurations after flow at 200-psi differential pressure.

35 percent of the rates from ideal perforations of the same size. Calculated CFE's for the same perforations in the linear system ranged from 65 to 85 percent.

Differences in perforation effectiveness between the two systems result from the fact that in the linear model most of the pressure drop occurs in the unpenetrated rock beyond the end of the perforation; hence the influence of the crushed zone is comparatively small. In the radial system, most of the pressure drop takes place across the crushed zone, making its influence substantially greater.

Unfortunately, the bare API sandstone core exposed to radial flow, as shown in Fig. 5, could not be used for experimental verification of radial-model calculations. Such a target would be shattered by the jet. A system that would permit evaluation of shot perforations was essential if the effects of the crushed zone were to be experimentally verified. Consequently, a radial-flow target that would withstand the shock of shooting tests was developed.

Experimental Radial Test System

To minimize modifications to existing laboratory facilities, it was decided to design the laboratory radial test system around the Berea sandstone target used in the API RP 43 test. However, the strong influence of the compacted zone indicated by radial-model flow calculations raised the question whether the observed crushed-zone configurations were peculiar to the highly confined 3⁹⁄₁₆-in.-diameter target. A series of shooting tests in targets ranging in diameter from 2½ to 6⅝ in. indicated no significant changes in compacted-zone configurations.

The mechanical support necessary to prevent the sandstone target from shattering during the jet penetration process was obtained by mounting the target in a steel housing in the standard API RP 43 fashion. Drilled perforation tests indicated that fluid could be introduced uniformly enough along the perforations through a series of radial holes drilled through the housing and cement. Various combinations of radial hole diameter and arrangement were evaluated. The system selected is shown in Fig. 7. It involves four rows of ⅜-in.-diameter holes drilled 25° above and below the axis of the bedding planes, with the individual holes within the rows longitudinally spaced 1.25 in. apart. This arrangement was economical, provided for adequate structural strength, and was found to be the most compatible with permeabilities derived from the Hassler measurements.[3,5] These permeabilities are necessary in determining the theoretical flow rates for comparison with measured rates in arriving at perforation-flow efficiency.

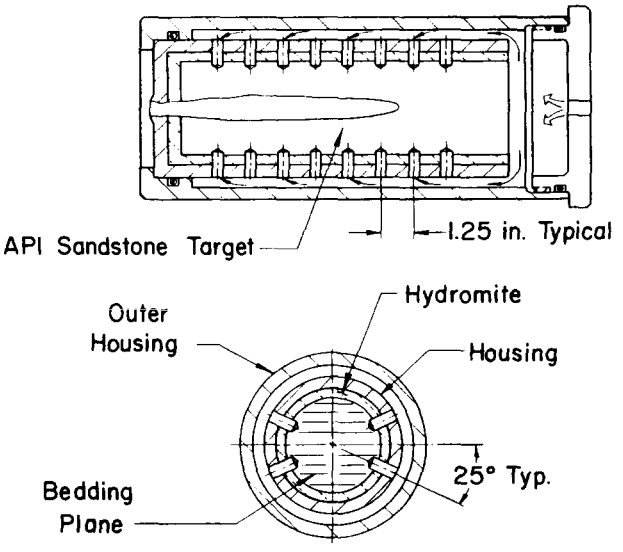

Fig. 7—Radial-flow test target.

Perforation Efficiency (PE) in the radial system of Fig. 7 is the ratio of flow rate from a shot perforation to flow rate from an ideal perforation of the same size under the same simulated reservoir conditions. To simulate the same conditions for shot and ideal perforations it was necessary to impose a higher differential pressure across the drilled-housing shooting target than that imposed across a bare core containing an ideal perforation of the same size. There are two reasons for this. First, the presence of the reduced-permeability crushed zone around the perforation results in higher pressures in the vicinity of the hole than in the case of an ideal perforation. Second, there is a pressure drop caused by the drilled-housing arrangement. This drop results from the reduced surface area of the target exposed to flow as compared with that area for a bare core.

Increased pressures caused by the presence of the crushed zones were calculated using Eq. A-3 for perforations having various diameters and depths, and having representative crushed zones. Although there was no way to calculate the pressure drop imposed by the limited core area exposed by the drilled housing, it was possible to determine it empirically. The procedure used is shown in Fig. 8. The pressures required on the 1.78-in.-radius ellipsoids to simulate various reservoir differentials were calculated using Eq. A-1 for various ideal perforation diameters and depths (Fig. 8a). Flow rates at these pressures were measured for bare targets containing drilled perforations (Fig. 8b). The cores were then sealed with Hydromite cement, and radial holes were drilled as discussed previously. The pressures that had to be imposed on the housing to provide flow rates equivalent to those from drilled perforations in bare cores were then measured (Fig. 8c), and the pressure drops imposed by the limited exposed area were determined.

As indicated earlier, the flow rates for perforations with crushed zones are lower than those for ideal perforations of the same size under the same simulated reservoir conditions. Since the housing-system pressure drop was proportional to flow rate, it was possible to determine the drops for perforation-crushed-zone systems of interest using the procedures set forth in Fig. 8. To determine the total pressures that had to be imposed across the target system, pressure-drop changes, corresponding to the reduced flow rates produced in the housing system by the presence of the crushed zone, were added to the increased pressures caused by the presence of the crushed zone. Pressure changes resulting from typical crushed zones and the drilled-housing arrangement are shown in

Fig. 9. It is apparent that the pressure required across the target approaches full reservoir differential regardless of perforation diameter or depth. For PE's of 40 percent or less, the maximum deviation from reservoir differential is less than 10 percent. Even if the PE's were as high as 60 percent, the deviation would be less than 14 percent. Consequently, full reservoir differential was imposed across the target to simplify testing, even though this would result in PE's measuring about 10 percent high.

An initial series of laboratory tests was made in the radial-flow test system at 200-psi differential pressure using shaped-charge guns of various sizes and types. PE's were determined as indicated above, and they were indeed found to be in the same range as had been calculated.

Comparative Flow Tests

A further series of tests was made to investigate the influence of varying differential pressure and shooting conditions (conventional positive pressure or expendable reverse pressure) on perforation-flow performance. The perforators selected for these tests were 2-in. and 3⅜-in. hollow carrier-type guns that represent, respectively, typical through-tubing and casing perforators.

Except for use of the radial-target system and a gas-over-liquid-accumulator arrangement for smooth flow in place of the reciprocating pump, tests were made in accordance with the standard API RP 43 test procedures.[3,5] The 3⅜-in. casing gun was tested under conventional completion (positive pressure) conditions. Differential pressure during the filtration phase was 500 psi for all tests. Backflow (from target to test well) was evaluated at differential pressures of 200, 100, 50, and 25 psi. Separate tests were performed at each pressure level, with the pressure being held constant throughout each test. The 2-in. through-tubing gun was tested under expendable (reverse pressure) conditions, with individual tests at constant differential backflow pressures of 500, 200, 100, and 50 psi, and under conventional (positive pressure) conditions with differential backflow pressures of 500 and 200 psi. Data from tests made in linear targets at standard API conditions are also included for comparison.

The influence of differential pressure on stabilized PE's in the radial-test system is shown in Fig. 10. Linear CFE's are also shown for the two charges. The data shown represent the average of several tests at each pressure level.

From Fig. 10, the standard linear CFE's indicate that the 2-in. gun perforations would flow at 76 to 84 percent of ideal capacity, depending on shooting conditions. However, the radial PE's for this gun are only 38 and 40 percent under the same conditions. For the 3⅜-in. gun the CFE is 72 percent compared with a PE of 29 percent at the same conditions. It can be seen that differential pressure has a significant effect on perforation efficiency for both charges. This is apparently the result of a reduced tendency to improve the permeability of the crushed zone at the lower differential pressures.

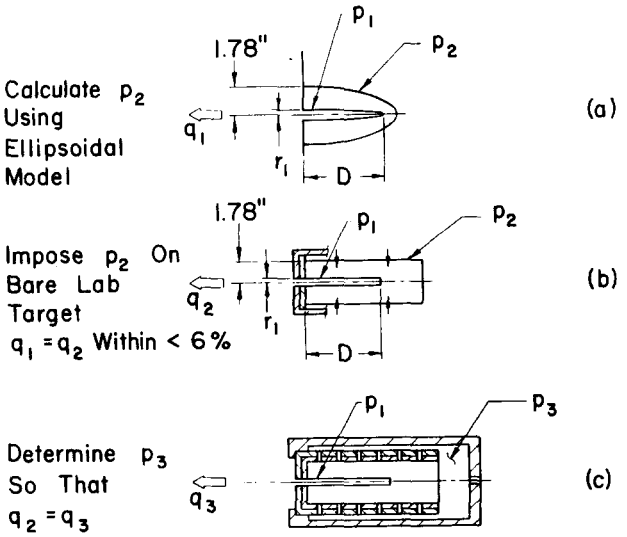

Fig. 8—Determining pressure drop across drilled housing.

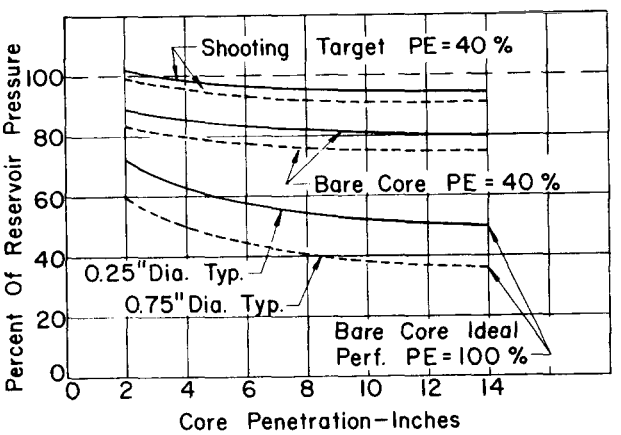

Fig. 9—Pressure imposed across radial target.

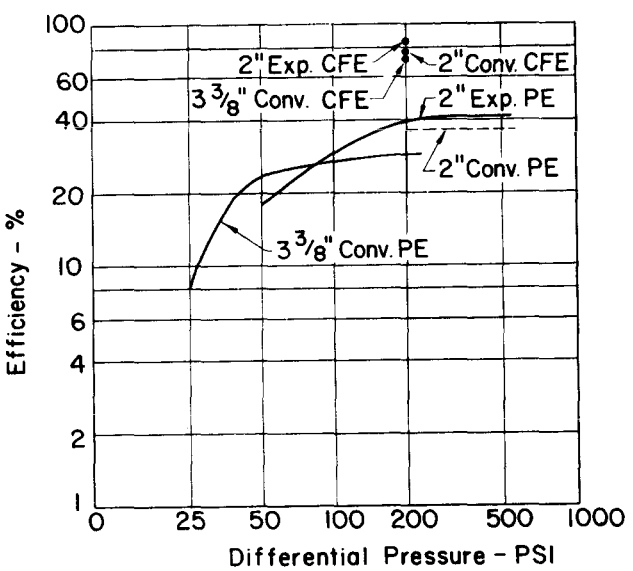

Fig. 10—Influence of differential pressure on perforation efficiencies. ("Conv." means hole pressure exceeds formation pressure. "Exp." means the reverse condition.)

PE increases with increasing differential pressure up to the 100- to 200-psi range for the 3⅜-in. charge and the 200- to 500-psi range for the 2-in. charge. It should be emphasized that the data presented pertain to liquid flow. As reported by other investigators, higher reverse differential pressures (up to several thousand psi) prove beneficial in gas-well completions.[7] The average PE for the 2-in. charge is slightly higher at 200 psi, regardless of completion conditions, than the PE for the 3⅜-in. perforator at 200 psi. As shown earlier in Fig. 6, the crushed zone for the 2-in. perforation is not so thick as that for the 3⅜-in. perforation, which would reduce the influence of the zone for the smaller charge.

It is interesting to note that there is little difference between the PE's observed under conventional and under expendable shooting conditions for the 2-in. gun. However, it must be remembered that the conventional tests were performed in accordance with the API test procedure,[3,5] and the filtration or invasion times were short — only a few minutes. Earlier studies[1,2] suggest that long-time invasion periods may change the picture significantly and weight the advantages in favor of expendable completion conditions.

Since differential pressure has a substantial effect on PE, its effect on flow rate is compounded, as indicated in Fig. 11. The rates have been corrected to standard conditions of viscosity and permeability. It is interesting that at 200 psi the flow rate of the 2-in. gun approaches that of the 3⅜-in. gun. Note the decay in flow rate with decreased differential pressure, with the 2-inch gun dropping more rapidly than the 3⅜-in. gun. Flow rates obtained in linear tests are shown to be substantially lower than the rates in the radial system.

The information shown in Figs. 10 and 11 represents the values of PE and flow rate after the perforations have been cleaned by flow. To achieve these levels requires from 10 to 50 liters of fluid, depending on charge size and level of differential pressure.

To understand more fully how perforations respond initially to the stimulus of flow, a study was made of PE and flow-rate increase with total volume of fluid flowed. These data are plotted in Figs. 12 and 13. PE is low at first and increases with flow through the perforation, eventually reaching a stabilized level. Tests indicated that, initially, the perforations are partially plugged with debris from the perforator and with crushed formation material. Typical perforations before flow are shown in Fig. 14. Essentially all of the visible solids that are expelled from the perforation are discharged very early in the clean-up process, generally in the first 1 to 2 liters of flow. From Figs. 12 and 13 it can be seen that the PE's are still low at this point. The subsequent increase in PE's apparently represents improvement of the crushed-zone permeability. This phenomenon was noted to the same degree in CFE buildup in linear tests.

That the perforation must be flowed to become effective is further demonstrated by Fig. 15, which presents the results of tests in which filtered kerosene was injected into the perforation immediately after shooting. Note that there is a decrease in flow from an already low initial value. The perforation was not effective for injection until the debris was removed and the crushed-zone permeability was increased through fluid flow. Other studies indicate that if the injection fluid is not absolutely clean, but contains particulate matter, the situation becomes even more unfavorable.[8]

The influence of the crushed zone is placed in better perspective when compared with the effects of variations in perforation diameter and depth. From the calculated data presented in Fig. 16 it can be seen that, for the specific perforation configuration chosen, the same increase in flow rate could be achieved by doubling the crushed-zone permeability as could be achieved by increasing the penetration about 60 percent. Increasing the hole diameter by a factor of approximately 2.5 would increase flow the same amount. Halving the crushed-zone thickness on the same perforation would increase the flow rate about the same amount as increasing penetration 25 percent or increasing hole diameter about 60 percent. Thus it can be seen that from the standpoint of flow

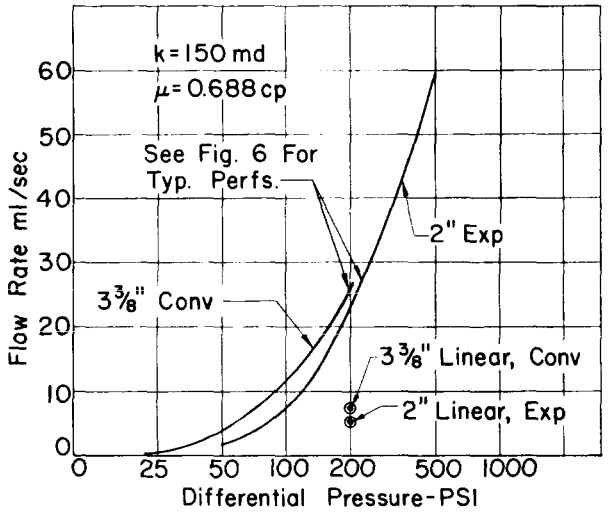

Fig. 11—Influence of differential pressure on flow rate.

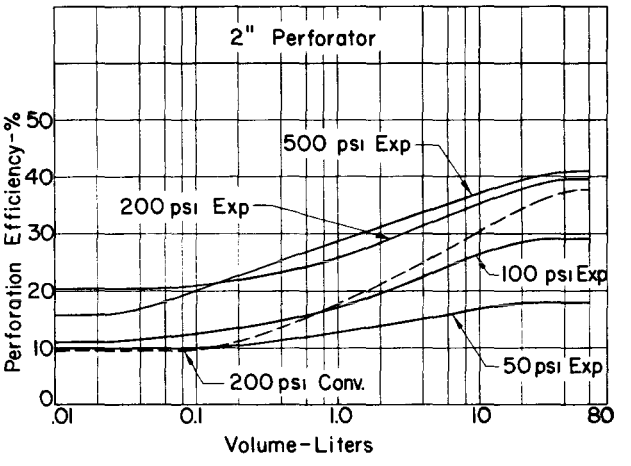

Fig. 12—Change in perforation efficiency with volume of backflow—2-in. perforator.

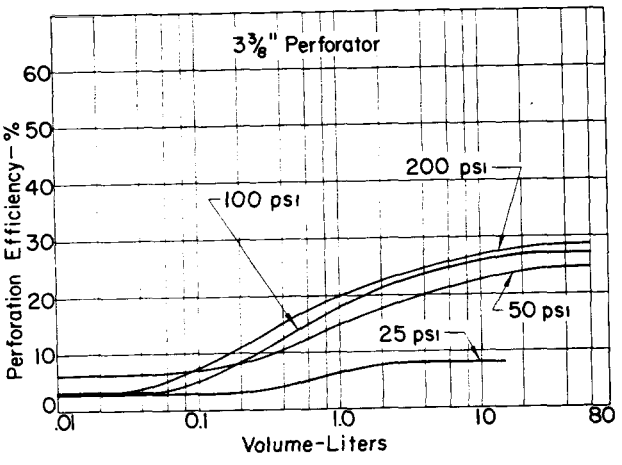

Fig. 13—Change in perforation efficiency with volume of backflow—3⅜-in. perforator.

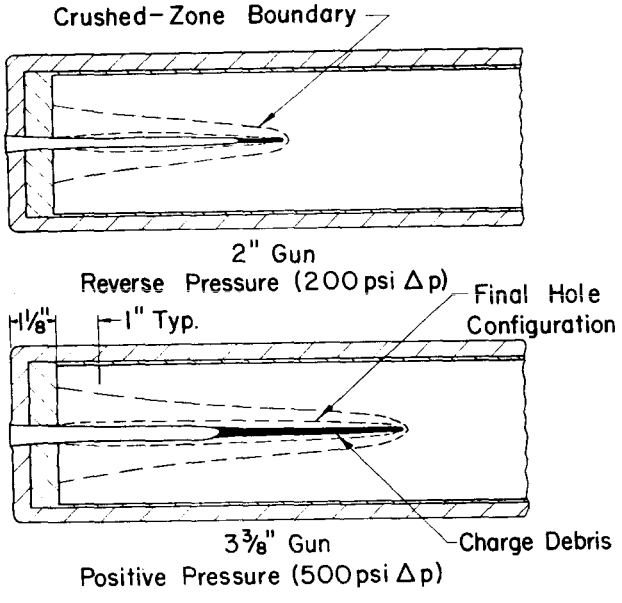

Fig. 14—Typical perforations before flow.

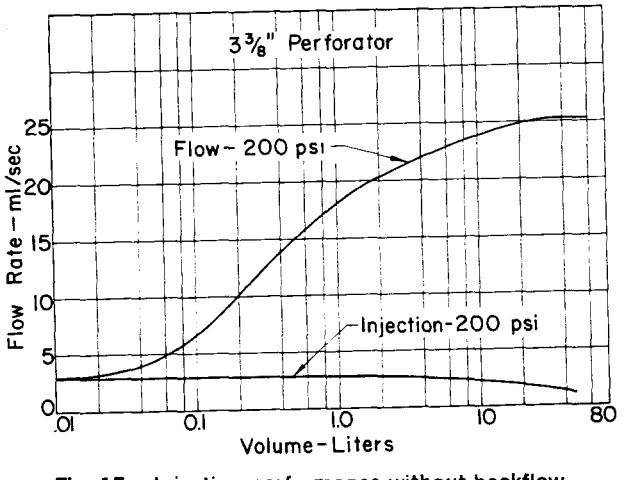

Fig. 15—Injection performance without backflow.

performance the crushed-zone characteristics of a perforation can be as important as its depth.

Implications for Field Application

We realize that the methods used in these studies simulate neither the effect of closely spaced multiple shots nor the effects of shot phasing, either of which can alter flow and pressure distributions. Only the Berea sandstone target was used in a clean-fluid environment. We also realize that perforation configurations vary from formation to formation,[9] and that tests in mud with longer invasion times could materially alter the results.[1,2] However, there are implications from these studies that will be useful in field completions.

Since the effectiveness of a perforation is sensitive to differential pressure, it would seem judicious to assure a high level of differential pressure toward the wellbore at the time of the perforating operation or at the time the perforations are flowed initially. This should enhance perforation efficiency and aid in getting more of the perforations in the system to begin flowing. As pointed out by previous investigations,[4,10,11] the productivity ratio of a well is governed by the number of perforations effective, this being more important than penetration — assuming the perforation extends a few inches past the damaged zone. This may be seen from Fig. 17, which indicates that a single perforation 12 in. deep is not so effective as four perforations only 2 in. deep in

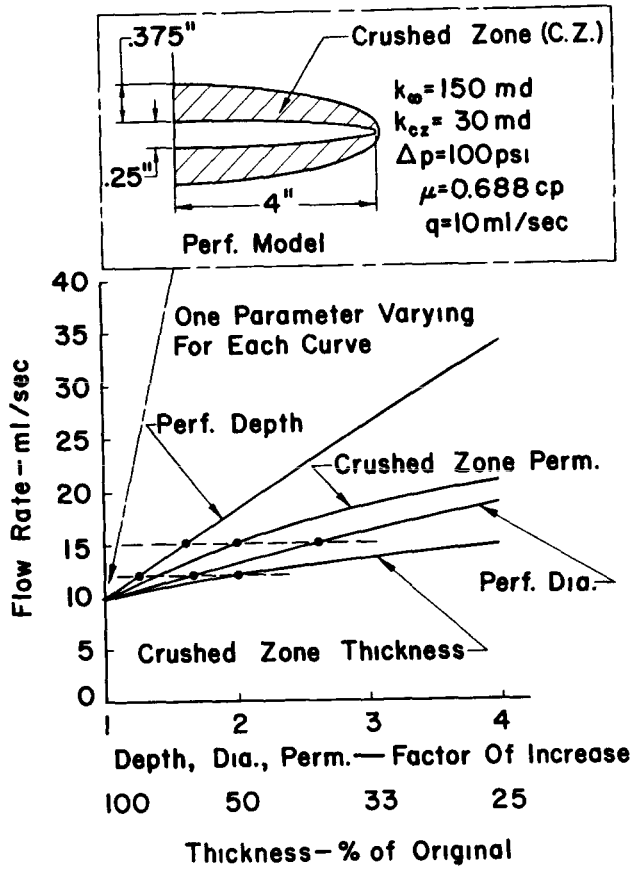

Fig. 16—Influence of different perforation parameters on flow rate.

the same formation interval. Of course, the information in Fig. 17 must be tempered by several considerations. It applies to blanket shooting at high shot densities. Penetration assumes greater importance for widely spaced shots, as indicated earlier in Fig. 4. Increased penetration is desirable, also, to reach beyond the area damaged by drilling fluids or cement filtrates. The plots in Fig. 17 are based on undamaged formations. Nevertheless, the importance of perforation efficacy is emphasized by the fact that wells perforated under reverse pressure with small guns having low penetration capacity often give better flow than wells shot under positive pressure with large guns providing deeper penetration.[12,13]

Should the low perforation-flow efficiencies observed in the radial tests apply to multidirectional, multishot completions in liquid-bearing formations, these very efficiencies raise the question of shot-density requirements for maximum productivity ratio, since the earlier investigators assumed ideal perforations in arriving at their data (Fig. 17).

As pointed out in earlier studies,[1,2] the problems of perforation clean-up are aggravated by the presence of mud. Often very high differentials were required to remove mud plugs, and even then perforation effectiveness was reduced. Although this information was developed in linear targets, it seems reasonable to assume that the situation will be similar under radial flow. The considerable possibility of reduced perforation efficiency would strongly suggest the use of compatible completion fluids. This is also borne out by field experience in which good perforation performance has been obtained by protecting perforations from mud with nonplugging completion fluids.[14,15]

The idea that perforations must be flowed before they can become effective also applies to injection systems. It appears desirable to backflow perforations at a high differential pressure before starting fluid injection.

Conclusions

The following conclusions and inferences are drawn that will doubtless suggest areas where additional work can be profitable.

1. Perforation-flow efficiencies are reduced by a low-permeability compacted zone that surrounds the perforation.
2. Perforation efficiencies in the radial-flow test system are substantially lower than those indicated by the linear API test.
3. Perforation efficiencies are strongly influenced by the level of differential pressure toward the wellbore, with efficiencies decreasing as differential pressure decreases.
4. Perforations are initially not very effective and are cleaned by flow. During flow, perforation-flow efficiency gradually increases to a maximum stabilized value. During perforation clean-up, most of the solids removed are quickly expelled, but flow efficiency is well below the maximum stabilized value at this time. Additional flow is required to increase the permeability of the crushed zone and thus increase perforation efficiency to a maximum.
5. Injection into perforations immediately after shooting and before they are flowed results in low injection efficiencies.

Nomenclature

A = cross-sectional area of medium perpendicular to lines of flow, sq cm
d = perforation diameter, in.
D = depth of perforation, in.
h = axial thickness of medium, cm
k = permeability of medium, darcies
k_{cz} = permeability of compacted zone, darcies
k_∞ = permeability of reservoir, darcies
L = length, cm
L_1 = distance from plane boundary to focal point of ellipsoidal perforation and all constant-pressure ellipsoids surrounding perforation, in.
L_2 = length of constant-pressure ellipsoid, in.
p = pressure
p_{cz} = pressure on surface of compacted zone, psi
p_e = pressure at outer radius of medium, atm
p_w = pressure at inner radius of medium, atm
p_1 = pressure on surface of perforation, psi
p_2 = pressure on surface of constant-pressure ellipsoid, psi
p_3 = pressure on outside of radial test target, psi
p_4 = upstream pressure, atm
p_5 = downstream pressure, atm
p_∞ = pressure at infinity (reservoir pressure), psi
q = flow rate, ml/sec
q_o = flow rate from uncased wellbore
q_p = flow rate from cased and perforated wellbore
q_t = calculated flow rate from ideal perforation, ml/sec
q_2 = measured flow rate from drilled perforation, ml/sec

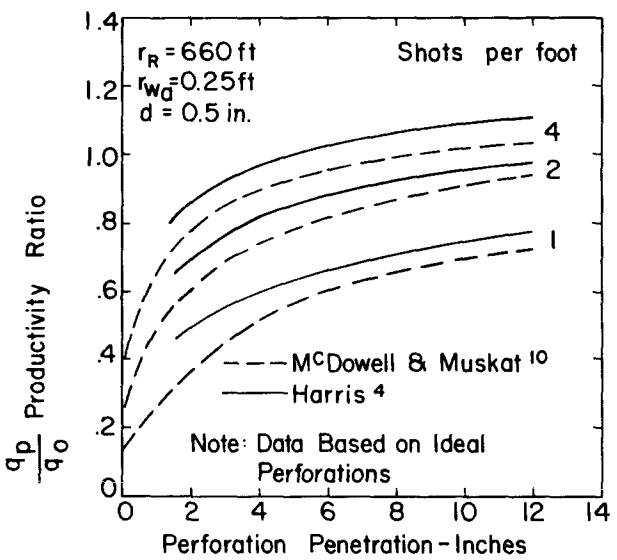

Fig. 17—Effect of shot density and penetration on productivity ratio.

q_3 = measured flow rate from shot perforation, ml/sec
r_e = outer radius of medium, cm
r_R = radius of reservoir, ft
r_w = inner radius of medium, cm
r_{wa} = radius of wellbore, ft
r_1 = perforation radius, in.
r_2 = radius of constant-pressure ellipsoid, in.
μ = viscosity of fluid, cp
ξ = constant defined by configuration of constant-pressure ellipsoid
ξ_{cz} = constant defined by boundary of selected crushed zone
ξ_1 = constant defined by boundary of perforation
ξ_2 = constant defined by configuration of specified constant-pressure ellipsoid

Acknowledgments

We wish to express our appreciation to J. H. Moran, J. J. Smolen and D. R. Fitch for their assistance in the development and application of the ellipsoidal perforation model and to H. C. Slider for his help in developing the mathematical model of the laboratory target.

References

1. Allen, T. O. and Atterbury, J. H., Jr.: "Effectiveness of Gun Perforating," *Trans.*, AIME (1954) **201**, 8-14.
2. Allen, T. O. and Worzel, H. C.: "Productivity Method of Evaluating Gun Perforating," *Drill. and Prod. Prac.*, API (1956) **207**, 112-125.
3. "Standard Procedure for Evaluation of Well Perforators," *API Recommended Practice 43*, API Div. of Prod., Dallas (Oct., 1962).
4. Harris, M. H.: "The Effect of Perforating on Well Productivity," *J. Pet. Tech.* (April, 1966) 518-528.
5. "Standard Procedure for Evaluation of Well Perforators," *API Recommended Practice 43*, second Ed. API Div. of Prod., Dallas (1971).
6. "Standard Procedure for Determining Permeability of Porous Media," *API Recommended Practice 27*, API Div. of Prod., Dallas (Aug., 1956).
7. White, W., Walker, T. and Diebold, J.: "A Proven Gas Well Completion Technique for Higher Deliverability," *J. Pet. Tech.* (June, 1965) 647-656.
8. Rike, J. L.: "Review of Sand Consolidation Field Experience in South Louisiana," *J. Pet. Tech.* (May, 1966) 545-550.
9. Thompson, G. D.: "Effects of Formation Compressive Strength on Perforator Performance," *Drill. and Prod. Prac.*, API (1962) **225**, 191-197.
10. McDowell, J. M. and Muskat, M.: "The Effect on Well Productivity of Formation Penetration Beyond Perforated Casing," *Trans.*, AIME (1950) **189**, 309-312.
11. Howard, R. A. and Watson, M. S., Jr.: "Relative Productivity Index of Gun Perforated Completions as Affected by Depth of Penetration," *World Oil* (Feb. 1, 1952) 166-172.
12. Huber, T. A. and Tausch, G. H.: "Permanent-Type Well Completion," *Trans.*, AIME (1953) **198**, 11-16.
13. Lebourg, M. P. and Hodgson, G. R.: "A Method of Perforating Casing Below Tubing," *Trans.*, AIME (1952) **195**, 303-310.
14. Priest, G. G. and Morgan, B. E.: "Emulsions for Use as Non-Plugging Perforating Fluids," *Trans.*, AIME (1957) **210**, 177-182.
15. Priest, G. G. and Allen, T. O.: "Non-Plugging Emulsions Useful as Completion and Well Servicing Fluids," *J. Pet. Tech.* (March, 1958) 11-14.

Original manuscript received in Society of Petroleum Engineers office Aug. 26, 1971. Revised manuscript received June 29, 1972. Paper (SPE 3444) was presented at SPE 46th Annual Fall Meeting, held in New Orleans, Oct. 3-6, 1971.

© Copyright 1972 American Institute of Mining, Metallurgical, and Petroleum Engineers, Inc.

APPENDIX

In the simplified down-hole system shown earlier in Fig. 2, the expression for the pressure along any ellipsoid is given by

$$p_2 = p_\infty - (p_\infty - p_1)\frac{\ln\left(\frac{\xi_2 + 1}{\xi_2 - 1}\right)}{\ln\left(\frac{\xi_1 + 1}{\xi_1 - 1}\right)}, \quad \ldots\ldots\ldots\ldots \text{(A-1)}$$

where ξ_2 and ξ_1 are constants determined by the configurations of the constant-pressure ellipsoid and the perforation, respectively. Total flow entering the perforation, as derived from the general Darcy relationship, is given by

$$q = \frac{0.691\pi L_1 k_\infty (p_\infty - p_1)}{\mu \ln\left(\frac{\xi_1 + 1}{\xi_1 - 1}\right)} \quad \ldots \text{(A-2)}$$

To determine the influence of the crushed zone on flow rates and pressure distributions in the ellipsoidal model, it is necessary to modify Eq. A-1 as follows:

$$p_{cz} = \frac{p_1 + p_\infty\left(\frac{k_\infty}{k_{cz}}\right)\left[\frac{\ln\left(\frac{\xi_1 + 1}{\xi_1 - 1}\right)}{\ln\left(\frac{\xi_{cz} + 1}{\xi_{cz} - 1}\right)} - 1\right]}{1 - \left(\frac{k_\infty}{k_{cz}}\right)\left[1 - \frac{\ln\left(\frac{\xi_1 + 1}{\xi_1 - 1}\right)}{\ln\left(\frac{\xi_{cz} + 1}{\xi_{cz} - 1}\right)}\right]}, \quad \ldots\ldots\ldots\ldots \text{(A-3)}$$

where p_{cz} is the pressure along the ellipsoid representing the surface of the crushed zone and ξ_{cz} is determined by the configuration of the ellipsoid defining the zone. This method assumes a crushed zone of uniform thickness in ellipsoidal coordinates. Using p_{cz} in Eq. A-1 in place of p_1, the pressure p at any point beyond the crushed zone can be calculated. The flows are also calculated substituting p_{cz} for p_1 and ξ_{cz} for ξ_1 in Eq. A-2 as indicated below:

$$q = \frac{0.691\pi L_1 k_\infty (p_\infty - p_{cz})}{\mu \ln\left(\frac{\xi_{cz} + 1}{\xi_{cz} - 1}\right)} \quad \ldots \text{(A-4)}$$

JPT